Mineralium Deposita (2026) 61:147–162
https://doi.org/10.1007/s00126-025-01382-8

ARTICLE

Genesis of the hot spring mercury deposits of the Mt. Amiata geothermal system (Italy) constrained by Hg and S isotope geochemistry

Paolo S. Garofalo[1] · Farshid Kiani[1] · Andrea Marchetti[2] · Lisa Lancellotti[2] · Orlando Vaselli[3,4] · Simone Beccari[5] · Gaetano Pedone[6] · Daniele Rappuoli[7]

Received: 3 January 2025 / Accepted: 4 July 2025 / Published online: 13 August 2025

Abstract

The world-class geothermal system of Mt. Amiata, Italy, comprises a district of 14 hot-spring cinnabar±stibnite deposits. We determined the Hg isotopic compositions of cinnabar and basement rocks of the geothermal system, coupled with S isotopic compositions of cinnabar, marcasite and stibnite, to constrain the source rocks in this geological environment. Most cinnabar, stibnite, and marcasite samples have $\delta^{34}S$ between −0.9 and +5‰. Cinnabar shows a relatively large range of $\delta^{202}Hg$ from −3.64 to +0.17‰ and $\Delta^{199}Hg$ from −0.43 to +1.06‰, although samples from individual deposits show much narrower $\delta^{202}Hg$ ranges. We interpret these values as the products of hydrothermal fractionation and mixing of magmatic, metamorphic, and marine sedimentary sources of Hg (Sb) and S, from which the samples inherited their signature. Comparison between the Hg isotopic signatures of the Mt. Amiata cinnabar and those of the world-class submarine geothermal systems of Almadén (Spain) and Idrija (Slovenia) shows significant differences. At Almadén and Idrija, the range of $\delta^{202}Hg$ values are typically < 2‰, while the corresponding values for Mt. Amiata have a much larger spread, similar to other geothermal systems in the western USA. This indicates notable differences between the range of fractionation processes occurring in submarine and continental geothermal systems.

Keywords Hot spring ore deposits · Mt. Amiata geothermal system · Mercury isotopes · Geothermal systems

Introduction

Geothermal systems are unique geological environments in which the circulation of hydrothermal fluids used for energy production occurs hand in hand with the formation of base- (Pb, Zn, Cu) and precious (Au, Ag) metal deposits (Au, Ag: Hedenquist and Lowenstern 1994; Brown and Simmons 2003; Simmons and Brown 2007; Hardardóttir et al. 2013; Barnes 2015). These deposits are commonly enriched in a group of by-product elements that are considered critical raw materials for modern industry (e.g., B, As, Sb, Ga, Ge: Various Authors 2023), but that are also potentially toxic pollutants (e.g., As, Sb, Hg, Tl: Zhang et al. 1998; Blum et al. 2014; Plant et al. 2014). All these occurrences show that, in order to be sustainably exploited, geothermal systems warrant comprehensive insights into the sources and sinks of all geothermal components.

A typical example of a geothermal metal that was intensely exploited in the past but that is currently ranked

Editorial handling: B. Lehmann

✉ Paolo S. Garofalo
paolo.garofalo@unibo.it

1 Dipartimento di Scienze Biologiche, Geologiche Ambientali, University of Bologna, Bologna, Italy

2 Department of Chemical and Geological Sciences, University of Modena and Reggio Emilia, Modena, Italy

3 Department of Earth Sciences, University of Florence, Firenze, Italy

4 Florence Unit, CNR-IGG Institute of Geosciences and Earth Resources, Firenze, Italy

5 Museo delle Miniere di Mercurio del Monte Amiata, Santa Fiora, Italy

6 Castel del Piano, Grosseto, Italy

7 Parco Nazionale Museo delle Miniere del Monte Amiata, Piancastagnaio, Italy

by the WHO (2017) as a priority pollutant is mercury (Hg). Mercury has active redox chemistry, forms covalent bonds with soft ligands (which generate stable sulfido complexes), is bioactive, and can be present as a volatile species (Hg^0) in hydrothermal fluids (Varekamp and Buseck 1984; Seward et al. 2014). Mercury has long been considered an indicator of hot springs ore deposits in active and fossil geothermal systems (e.g., New Zealand, California) and was mainly documented in the form of Hg sulfides (cinnabar or metacinnabar, both HgS) and metallic Hg (Davey 1974; White 1981; Barnes and Seward 1997). Such enrichment in hot springs is considered the final segment of a larger crustal cycle that involves initial stages of mobilization from source rocks and transport by hydrothermal fluids, and final stages of dispersal into the lithosphere, hydrosphere, and atmosphere.

A key method used to quantify Hg sources and sinks is the determination of isotope compositions (Lepak et al. 2015; Washburn et al. 2018). Mercury is a heavy element (200.6 g/mol) with seven natural stable isotopes (^{196}Hg, $^{198–202}$Hg, ^{204}Hg) that display both mass-dependent and mass-independent fractionation (Bergquist and Blum 2007, 2009). The most typical mass-dependent fractionation (MDF) is measured by even-mass-number isotopes and is usually defined as the ‰ deviation of $^{202}Hg/^{198}Hg$ relative to the NIST SRM 3133 Hg standard (δ^{202}Hg). The less typical mass-independent fractionation (MIF) is generated by nuclear volume or magnetic isotope effects in photochemical reactions of Hg species in the near-surface environment. It is determined by odd-mass-number isotopes and is expressed as Δ^{199}Hg (Bergquist and Blum 2009). Because these distinct types of fractionation are due to fundamentally different chemical mechanisms, they have been used to define biotic vs. abiotic Hg processes. Hence, Hg isotopic compositions are used not only to identify pristine earth reservoirs, but also to constrain biogeochemical processes.

In this work, we present a dataset consisting of Hg and S isotope compositions on an important Hg historical mine district, i.e. the Hg(±Sb) district associated with the geothermal system of Mt. Amiata, Italy (Fig. 1). This district is a Hg reservoir of global importance because it produced in total c. 117,000 t of Hg (Segreto 1991) during a mining history that lasted for nearly one and half century (from 1846 to 1982, Tanelli 1983).

A recent study on this continental geothermal system (Pribil et al. 2020) reported a dataset on Hg isotope ratios from two deposits of the district, sediment, soil, fish, geothermal water, geothermal precipitate, and calcine (i.e., residues produced from ore retorting). These data were used to constrain the cycling of Hg in the Amiata environment. In this study, we present the Hg isotope compositions of cinnabar samples from eight (out of fourteen) deposits of the Mt. Amiata geothermal system and of basement rocks of the geothermal reservoir. We combine these data with δ^{34}S data of cinnabar, stibnite, and marcasite to show that the ranges of δ^{202}Hg, Δ^{199}Hg, and δ^{34}S of these sulfides likely reflect a combination of hydrothermal fractionation and mixing of distinct Hg and S sources in which the magmatic source is dominant. This dataset provides useful insight into Hg cycling in similar continental hydrothermal systems.

The Mt. Amiata geothermal system

The geothermal system of Mt. Amiata (Fig. 1) is an important energy resource of Italy (Gianelli et al. 1988; Batini et al. 2003). With its heat flow exceeding 300 mW m^{-2} (Fulignati et al. 2014), this system hosts today five power plants that exploit two geothermal reservoirs to generate 121 MWe power capacity (Bertani 2016).

This geothermal system formed within the Northern Apennine thrust-and-fold belt and had a complex tectonic evolution (Marroni et al. 2015a; and ref. therein) that was crucial for its genesis. In short, the geological setting of this system was defined by the generation of a thick, E-NE-verging stack of nappes during continental collision in the Miocene (Faccenna et al. 2001). Subsequent to collision, the nappe stack started collapsing due to a stage of extensional tectonics (Carmignani et al. 1994; Jolivet et al. 1998) during which a set of horst and graben structures formed (Cataldi 1967). Until the end of the Neogene period, these structures were filled by poorly permeable, continental and marine sediments (Martini and Sagri 1993; Cornamusini et al. 2011). The evidence for extension affecting the Mt. Amiata area is mostly based on a large geophysical dataset (e.g., Chiarabba et al. 1995; Della Vedova et al. 2001; Cassinis et al. 2005). This dataset was coupled with available petrological data on the magmatic rocks of the region (Peccerillo et al. 2001; Peccerillo and Donati 2003; Conticelli et al. 2010) and with drill hole data from geothermal exploration (Pandeli et al. 1988; Elter and Pandeli 1991; Brogi 2008) to build a comprehensive tectonic model of southern Tuscany and Mt. Amiata in particular (Marroni et al. 2015a). Based on this model (Fig. 2), a volcano-plutonic complex formed at Mt. Amiata (Cadoux and Pinti 2009; Conticelli et al. 2015), which affected the nappe stack and the Neogene sedimentary deposits. The pluton is probably located at a depth of 5–6 km, has a laccolith shape (Acocella 2000; Acocella and Mulugeta 2001), and was emplaced starting approximately from the Lower Pliocene. The volcano is made of trachydacitic to olivine-latitic lava flows and domes, which were emplaced between 305 and 231 ka ago (Cadoux and Pinti 2009; Conticelli et al. 2015). The Upper Paleozoic-Middle Triassic basement rocks– the so-called Tuscan Metamorphic

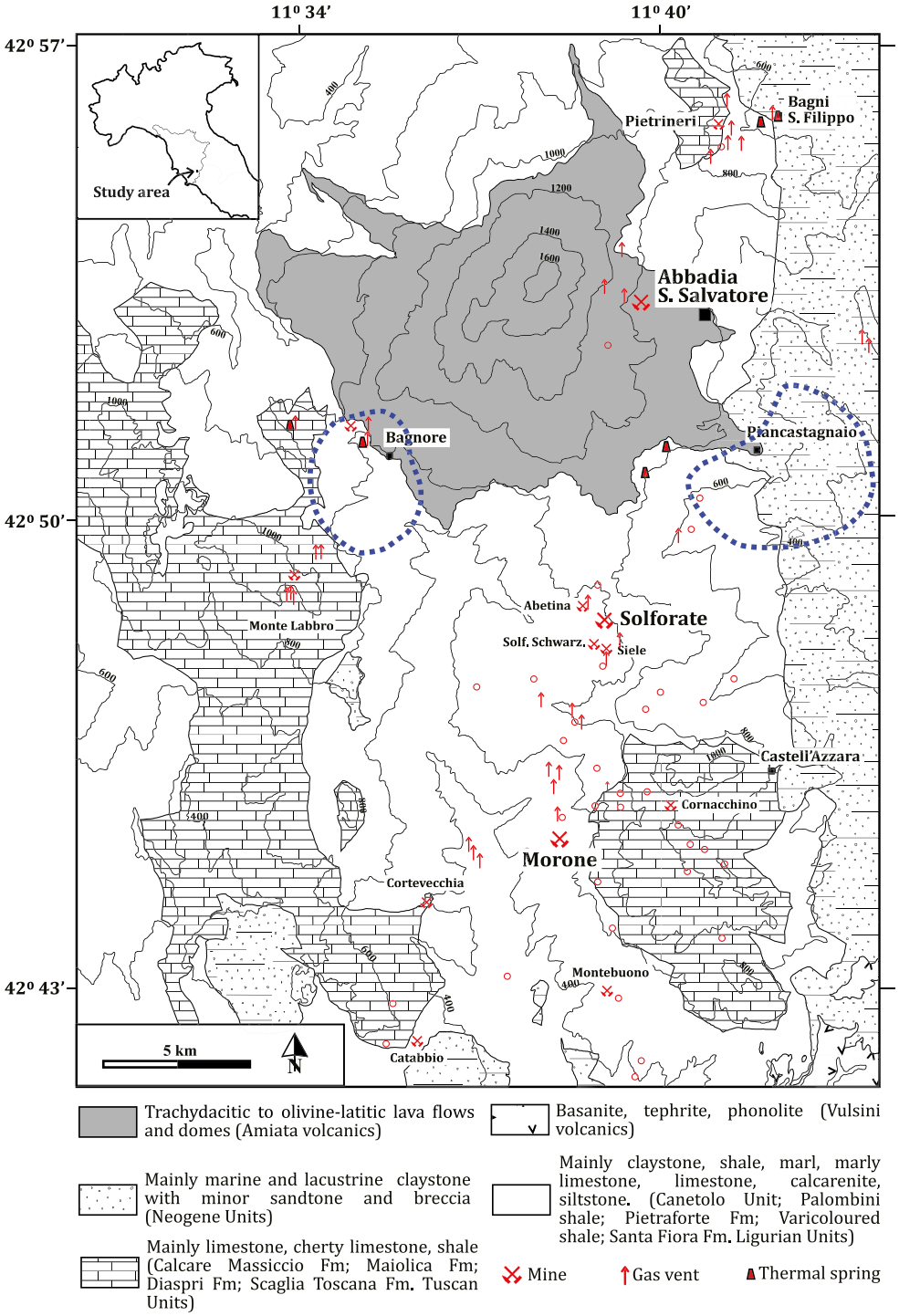

Fig. 1 Schematic geological map of the Mt. Amiata geothermal system and distribution of the associated cinnabar±stibnite mines, hot springs, and gas vents (modified after Calamai et al. 1970). The thick dotted lines mark the areas of geothermal power production (from: Barelli et al. 2010). Structural features are not reported for simplicity. The three largest mines of the district are shown with larger letters. The inset shows the district location in southern Tuscany

Complex – are a monotonous sequence made of graphite-rich phyllite and greywacke of low metamorphic grade, graphite-bearing marble, and hematite-, chlorite-, and anhydrite-bearing phyllite and dolostone. The basement rocks do not outcrop in the study area (Fig. 1), but in the drilled locations they have a thickness exceeding 3000 m (Barelli et al. 2010). This basement complex outcrops about 40 km northwest of Mt. Amiata along the Farma river (not in Fig. 1), where it occurs as a c. 800 m-thick sequence of fine- to coarse grained greywacke, siltstone, graphite-rich phyllite, bioclastic limestone breccia, and conglomerate (Farma schist, Gianelli et al. 1988; Engelbrecht 2008).

The geothermal system is made of two wet-steam (i.e., two-phase) reservoirs (Batini et al. 2003; Barelli et al. 2010; Marroni et al. 2015a). The shallowest is located at 500–1000 m depth (T: 150–200 °C) within the Mesozoic

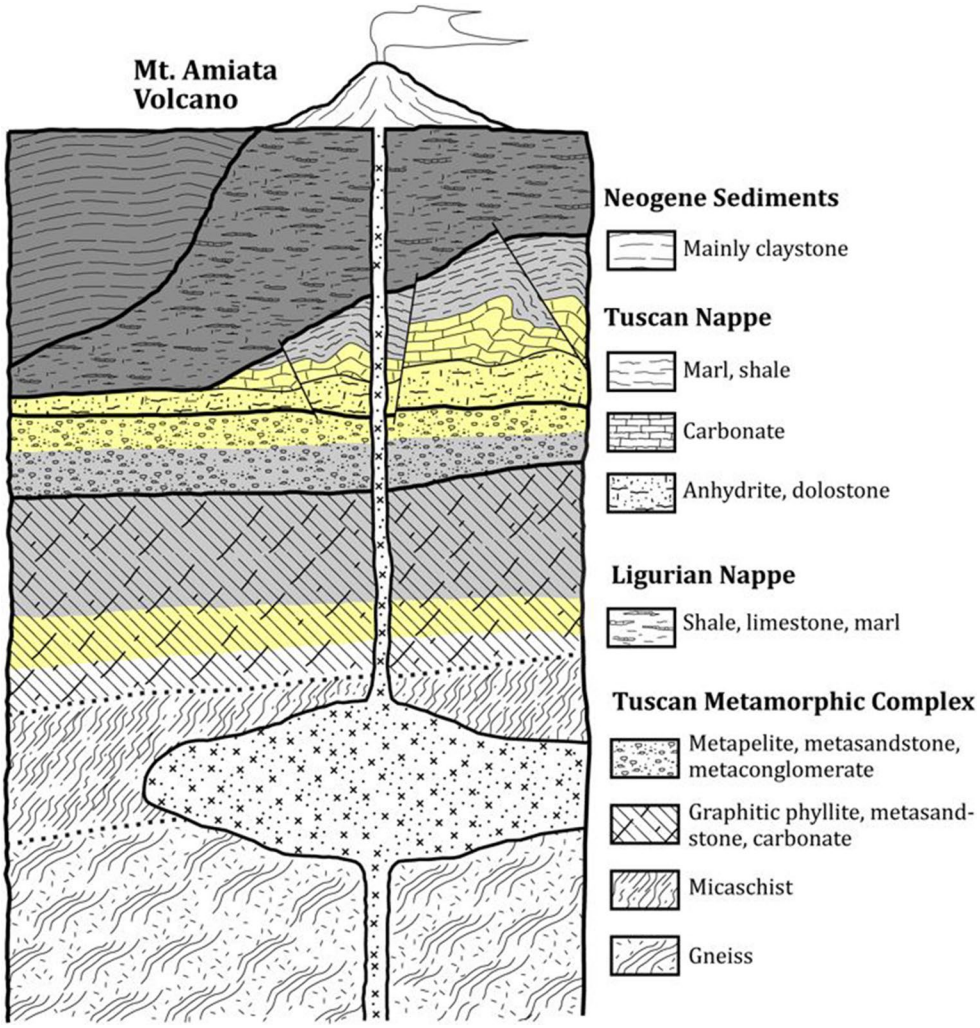

Fig. 2 Schematic tectonic model of Mt. Amiata (not to scale) showing the relations between the volcano-plutonic system and the local thrusted-and-folded structure of the Apennine belt (modified after Barelli et al. 2010). Highlighted in yellow are the two geothermal reservoirs as defined by geothermal exploration. The grey tones superposed to the shallow lithologies mark the impermeable caprock of the geothermal system

carbonates and Late Triassic evaporite rocks (anhydrite, dolostone) of the Tuscan Units and within the metapelite, metasandstone and metaconglomerate of the Tuscan Metamorphic Complex, which form cataclastic levels of the nappe stack (Fig. 2). The deepest reservoir is at about 3000 m (T: 300–360 °C) within the relatively permeable levels of the Tuscan Metamorphic Complex.

The caprocks of the geothermal system are the poorly permeable claystone, shale, marl, siltstone, sandstone, and limestone of early Cretaceous-Eocene age deposited onto the Piedmont-Ligurian oceanic basin (Marroni et al. 2015b) and forming the Ligurian Unit of the nappe stack (Figs. 1 and 2). Other caprocks are the shallow marine to lacustrine claystone and conglomerate of Neogene age (Bonciani et al. 2005).

The Hg (±Sb) ore deposits of Mt. Amiata are associated with hot springs and gas vents (Fig. 1) and occur in a region of >450 km^2. The historical significance of these deposits is highlighted by a USGS report issued after World War II (Meyer and Mitchell 1947), which identified Italy as a leading global producer and the ore grades and reserves of the Amiata district as "enormous" if compared with those of the American continent. The ore bodies consisted of cinnabar, marcasite, pyrite, and minor stibnite hosted by rocks belonging to both the Tuscan and Ligurian Units (Table 1; Figs. 1 and 2). Sedimentary (Zucchetti 1964a; Arisi Rota et al. 1971) and geothermal (Morteani et al. 2011) constraints indicate that the mineralizing event could have started in the Late Pliocene and is still ongoing today, identifying an exceptionally long hydrothermal event. In the entire district, the most important gangue mineral in addition to clay minerals is calcite, while dawsonite, amorphous silica (opal, chalcedony), quartz, celestine, fluorite, gypsum, and zeolites are minor phases. These deposits were recently interpreted as modern analogues of Carlin-type epithermal deposits (Sillitoe and Brogi 2021).

Table 1 Summary of geological features of the Hg (±Sb) deposits from the Monte Amiata district

Mine	Host rocks	Ore body	Ore minerals	Gangue
Abbadia S. Salvatore	Calcarenite and calcilutite (Nummulitic limestone - Eocene)	Chaotic and disseminated. Stockwork. Vertically continuous, funnel-shaped breccias (chimneys)	Cinnabar, metacinnabar, pyrite, marcasite	Calcite, clay
Solforate Schwarzenberg	Sandstone and calcilutite (Eocene)	Chaotic and disseminated	See Solforate	See Solforate
Solforate	Sandstone and calcilutite (Eocene)	Veins, disseminations within clays. Replacement bodies within calcarenites	Cinnabar, pyrite, marcasite, stibnite	Clay, calcite, gypsum, quartz, dawsonite
Morone (Selvena)	Anhydrite rock, dolostone, black limestone (Rhaetian)	Stratabound, disseminated, chaotic. Vertically continuous funnel-shaped breccias (chimneys)	Cinnabar, pyrite, stibnite	Clay (black), gypsum
Siele	Calcarenite and calcilutite (Eocene)	Stockwork (vein thickness: up to 20–30 cm)	Cinnabar, marcasite	Clay (black), calcite, bitumen
Abetina	Calcarenite and calcilutite (Eocene)	Stockwork	Cinnabar	
Cornacchino	Limestone and radiolarite (Lower Cretaceous)	Chaotic masses embedded within limestone and cm-thick stockwork within radiolarites	Cinnabar, pyrite	Clay (black, yellow), gypsum, calcite, silica
Cerreto Piano	Sandstone (Pliocene)	Stratabound disseminations and concretions	Cinnabar	-
Bàgnore	Sandstone (Upper Cretaceous Pietraforte)	Stockwork veins and stratabound replacement of sandstone levels	Cinnabar, metacinnabar, mercury, pyrite, marcasite, goethite	Calc, gypsum
Bagni S. Filippo (Pietrineri)	Dolostone (Rhaetian). Limestone (Lower Jurassic)	Cinnabar grade increases with depth	Cinnabar	Clay, celestine, gypsum
Montebuono (Reto)	Calcarenite (Nummulitic limestone - Eocene)	Disseminations. Vertically continuous, funnel-shaped breccias, mainly at contact with shales	Cinnabar	Clay, Fe-oxides
Cortevecchia	Calcarenite, (Nummulitic limestone - Eocene)	Chaotic, developed at contact with shales. Vertically continuous, funnel-shaped breccias	Cinnabar, pyrite	Native S, dawsonite
Catabbio	Marl and claystone (Galestro)	Disseminations and thin films within faults and argillic alteration	Cinnabar, pyrite, marcasite	Calcite, quartz
Monte Labbro	Limestone (Lower Jurassic)	Replacements and disseminations within radiolarite (Diaspri) and Maiolica limestone (Neocomian)	Cinnabar	-

Data compiled from De Ferrari (1890); De Castro (1914); Savoia (1919); Zucchetti (1964a); Baccos (1967); Arisi Rota et al. (1971 Strappa (1977a, b, c); Schavecher (1990); Forconi (2011) and integrated with own data from Abbadia S. Salvatore. Notice that documentation on clay mineral compositions from the gangue assemblage is incomplete and defined in only few deposits

Materials and methods

Due to the difficulty of sampling cinnabar samples from the pristine ore bodies (which are not accessible anymore for environmental and safety reasons), all the studied material was selected from museums (Parco Museo Minerario di Abbadia S. Salvatore; Museo delle Miniere di Mercurio del Monte Amiata) and private collections. Samples were selected according to their freshness and representativeness, i.e., to the degree to which they showed the typical ore mineral assemblage of the pristine mines (Table 1). This selection allowed focusing on 23 samples from distinct ore deposits of Mt. Amiata (Fig. 3). Since only a few samples were originally tagged with geographic coordinates and depth, information on their exact locations within the pristine ore bodies is limited.

In detail, the cinnabar samples are representative of eight mines (Figs. 1 and 3; Table 1), which include the two largest mines of the district (i.e., Abbadia S. Salvatore and Solforate, which provided c. 75% of the historical Hg production: Strappa 1977c), a medium-sized mine (Morone), and five minor mines (Cortevecchia, Cerreto Piano, Monte Labbro, Bàgnore, and Cornacchino). Notably, samples from Cerreto Piano (Fig. 3f) are included in this study because of the historical relevance of this deposit reported in the local literature (Forconi 2011) although this deposit is located outside the area of the geothermal system shown in Fig. 1, about 16 km southwest of the Catabbio mine. Samples Abbadia 14, 10a, 10c, 8b, 6, 5a, and 2a were collected at Abbadia San Salvatore in the mine levels −200, −125, −75, −25, Serdini, XXII, and XI (Table 2), respectively, which correspond to a vertical interval of about 450 m in the mine (ESM, Fig. 1).

Two additional samples from a representative outcrop of the phyllite and quartzite of the Tuscan Metamorphic Complex (Farma Schists, samples MR1 and MR2) were collected along the Farma river close to the locality called

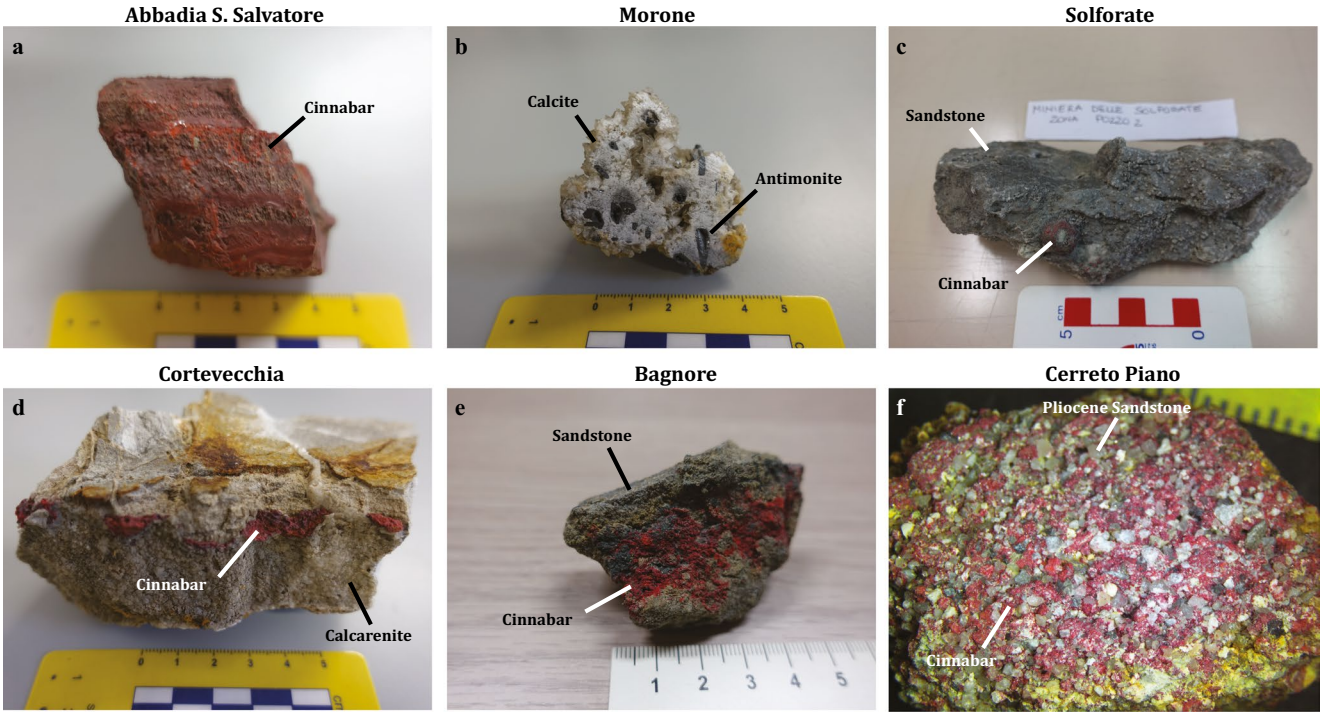

Fig. 3 Selected Mt. Amiata cinnabar samples used for this study. Samples from the largest (**a**, **b**, **c**) and smaller mines (**d**, **e**, **f**) of the district were selected in order to show the largest possible variety of cinnabar-stibnite occurrences. These include massive mineralizations (**a**), stibnite mineralization (**b**, only at Morone), disseminations (**e**, **f**), and veins (**d**). A peculiar cinnabar occurrence is the spherulitic aggregate of small crystals called "strawberry" (c)

Solaia, 40 km NW of Mt. Amiata (WGS84 coordinates - E: 11°0.256669; N: 43°0.082942). At the outcrop scale, this schist is massive and does not show evidence of veining or hydrothermal alteration. Samples MR1 and MR2 are fine grained shale that were used in a previous study on the petrochemical characterization of the Tuscan Metamorphic Complex (Agostini 2018). They can be considered representative of a basement lithology that did not experience hydrothermal overprint. Before analysis, all samples were individually screened with a binocular microscope and later used for petrographic documentation using a Nikon Eclipse Ci-POL microscope. The samples were crushed manually in an agate mortar and hand-picked to separate cinnabar, stibnite, and marcasite from the host rocks and gangue minerals. In most samples, two aliquots of these minerals were prepared to allow coupled measurements of Hg and S isotopes.

The Hg isotopes were measured at the University of Modena and Reggio Emilia using a multi-collector inductively coupled plasma-mass spectrometer (Neptune, Thermo Fisher Scientific, Bremen, Germany) equipped with a cold vapor generator and a desolvating apparatus as sample introduction system. The analytical method was optimized to obtain a suitable data precision while consuming a small sample volume (~4mL per run) fitting the sample loading loop. A detailed account of the analytical procedure of Hg isotope measurements is given in ESM 1, which provides details on the operating conditions, sample treatment, and solution preparation. The accuracy of the analytical procedure was tested by measuring the isotopic compositions of two reference materials (PACS-2 marine sediment and MA-4 cinnabar) whose compositions are in excellent agreement with the established reference values (ESM Tables 4 and 5). The precision of the isotope ratios was evaluated by repeating the isotopic compositions of three samples in distinct runs, which showed very good reproducibility of the measurements (ESM Table 6). Accuracy of the δ^{202}Hg (‰) data is 0.10‰ (2s).

The Hg-MDF isotope ratios are expressed in ‰ with the δ^{xxx}Hg notation as:

$$\delta^{xxx}\mathrm{Hg}\ (‰) = \left[\left({}^{xxx}\mathrm{Hg}/{}^{198}\mathrm{Hg}_{\mathrm{sample}}\right) / \left({}^{xxx}\mathrm{Hg}/{}^{198}\mathrm{Hg}_{\mathrm{standard}}\right) - 1)\right] \times 1000$$

where ^{xxx} denotes the 199, 200, 201, or 202 isotopes.

We use the conventional δ^{202}Hg to evaluate MDFs (Bergquist and Blum 2007). The Hg-MIF isotope ratios are reported by the Δ notation, which identifies the difference between the measured and predicted δ^{xxx}Hg, in ‰ units. The expression is:

$$\triangle^{xxx}\mathrm{Hg} = \delta^{xxx}\mathrm{Hg} - \delta^{202}\mathrm{Hg} \times \beta$$

Table 2 Mercury and sulfur isotopic compositions of the samples studied

Sample	δ^{199}Hg	δ^{200}Hg	δ^{201}Hg	δ^{202}Hg	Δ^{199}Hg	Δ^{200}Hg	Δ^{201}Hg	Cin	Mrc	Sbn	Altitude, mine level
								δ^{34}S			
	‰										m
Abbadia 10c	0.00	0.04	0.08	0.10	−0.03	−0.01	0.00	0.50	-	-	512, −200 m Level
Abbadia 10a	−0.06	−0.70	−1.29	−1.72	0.37	0.17	0.00	-	-	-	512, −200 m Level
Abbadia 14	0.18	0.26	−0.08	0.10	0.15	0.21	−0.15	−0.90	-	-	587, −125 m Level
Abbadia 8c	-	-	-	-	-	-	-	-	3.50	-	637, −75 m Level
Abbadia 8b	−0.12	−0.04	0.08	0.17	−0.16	−0.13	−0.05	2.30	-	-	637, −75 m Level
Abbadia 6	−0.18	−0.22	−0.30	−0.30	−0.10	−0.06	−0.08	1.00	-	-	687, −25 m Level
Abbadia 5a	−0.30	−0.52	−0.61	−0.81	−0.09	−0.11	0.00	−0.40	-	-	712, Serdini Level
Abbadia 11a	-	-	-	-	-	-	-	-	1.47	-	888, VII Level
Abbadia 2a	−0.36	−0.96	−1.22	−1.62	0.05	−0.14	0.00	1.80	-	-	905, XXII Level
Abbadia 1	-	-	-	-	-	-	-	−0.30	-	-	960, XI Level
Abbadia 1*	-	-	-	-	-	-	-	−0.40	-	-	960, XI Level
Morone 3	−0.71	−1.78	−2.89	−3.24	0.11	−0.15	−0.46	10.10	-	-	-
Morone 2	−0.65	−1.17	−2.13	−1.92	−0.17	−0.20	−0.68	11.60	-	-	-
Morone a	−0.59	−0.69	−1.45	−0.81	−0.39	−0.29	−0.84	-	-	0.80	-
Solforate	−0.41	−0.48	−1.14	−0.61	−0.26	−0.17	−0.69	3.55	-	-	-
Solforate Pozzo 2	−0.47	−0.35	−0.91	−0.17	−0.43	−0.26	−0.79	5.00	-	-	-
Cortevecchia 2	−0.89	−1.43	−2.21	−2.13	−0.35	−0.36	−0.61	−0.10	-	-	-
Cortevecchia 4	−0.47	−0.52	−1.22	−0.54	−0.34	−0.25	−0.81	−12.80	-	-	-
Cerreto Piano 1	−0.47	−0.43	−1.07	−0.37	−0.38	−0.25	−0.79	−6.80	-	-	-
Cerreto Piano 2	−0.59	−0.82	−1.60	−1.11	−0.31	−0.26	−0.76	−5.80	-	-	-
Cerreto Piano 3	−0.65	−0.82	−1.52	−0.98	−0.41	−0.33	−0.79	−4.65	-	-	-
Monte Labbro	−0.47	−0.35	−1.07	−0.24	−0.41	−0.23	−0.89	−12.50	-	-	-
Monte Labbro 2	0.24	−0.61	−2.05	−3.2	1.04	1.00	0.35	−6.90	-	-	-
Bàgnore	0.36	−0.30	−1.52	−2.52	0.99	0.96	0.38	-	-	-	-
Cornacchino 1	−0.06	−0.91	−1.98	−3.2	0.75	0.70	0.43	-	-	-	-
Cornacchino 2	0.24	−0.61	−2.05	−3.26	1.06	1.03	0.4	-	-	-	-
Cornacchino 3	0.00	−0.91	−2.28	−3.64	0.92	0.92	0.45	-	-	-	-
MR1 schist	−1.36	−2.56	−2.13	−3.61	−0.45	−0.75	0.58	-	-	-	-
MR2 schist	−0.77	−1.82	−1.98	−2.94	−0.03	−0.35	0.23	-	-	-	-

where β is equal to 0.2520, 0.5024, and 0.7520 for Δ^{199}Hg, Δ^{200}Hg, and Δ^{201}Hg, respectively (Bergquist and Blum 2007). The accuracy of the Δ^{199}Hg values is 0.04‰ (2s).

The S isotope ratios were determined by Activation Laboratories Ltd., Ancaster, Ontario, Canada. Twenty-two aliquots of cinnabar, stibnite, and marcasite samples were used for these measurements. These aliquots were split from the same samples used for the Hg isotope measurements. Analyses were carried out with a Mat 253 Thermo Scientific isotope ratio mass spectrometer coupled with a Fisons Instruments element analyzer to measure ^{34}S-SO_4, for which standards NBS 127 ($\delta^{34}S$: +21.12 ± 0.22‰), IAEA SO5 ($\delta^{34}S$: +0.5 ± 0.2‰), and IAEA SO6 (Ba sulfate, $\delta^{34}S$: −34.1 ± 0.2‰) were used. Individual analyses were conducted on about 3 mg mass of dry sample, which was mixed with c.3 mg of Nb_2O_5 and later combusted at 980 °C within the element analyzer. The released pure SO_2 was then transported by a He flux into the mass spectrometer for analysis. Data were corrected and normalized, and the results are expressed in the $\delta^{34}S$ notation. Table 2 reports the Hg and S isotopic compositions of all samples studied.

Results

The cinnabar samples exhibit a large range of δ^{202}Hg values between −3.64 and +0.17‰ and Δ^{199}Hg values between −0.43 and +1.06‰ (Fig. 4a). However, samples from individual deposits show a range of δ^{202}Hg that is much narrower than that of the entire dataset. No systematic variations of δ^{202}Hg and Δ^{199}Hg are evident as a function of geographical location or depth within the ore bodies (i.e., samples 10–2a of Abbadia S. Salvatore, Table 2). Notably, 13 out of 23 samples belonging to Abbadia S. Salvatore, Solforate, Morone, Cerreto Piano, Cortevecchia, and Mt. Labbro have δ^{202}Hg between −1.11 and +0.17‰ (Fig. 4a). These samples show Δ^{199}Hg ranging between −0.41 and +0.15‰. The 10 samples having more negative δ^{202}Hg between −3.64 and −1.62‰ (from Abbadia S. Salvatore,

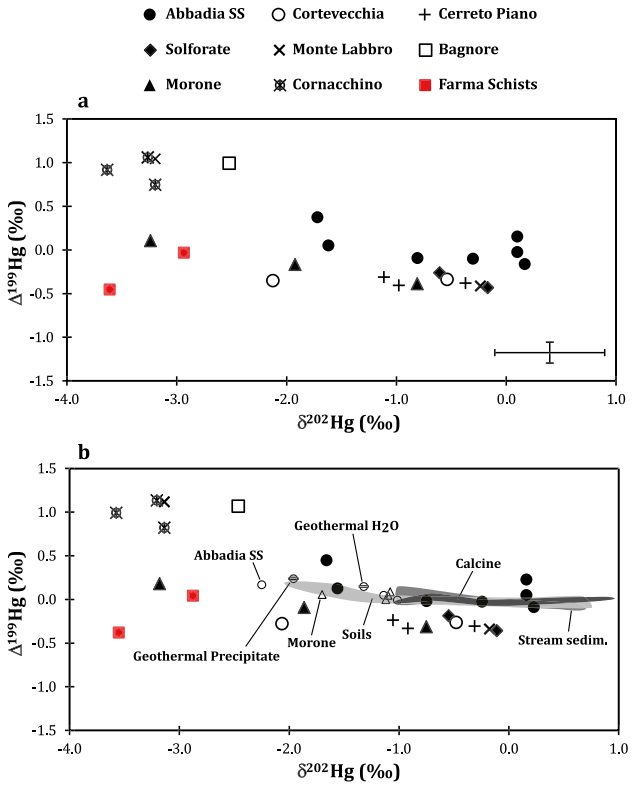

Fig. 4 Mass dependent fractionation (δ^{202}Hg) vs. MIF (Δ^{199}Hg) determined for the analyzed samples. (**a**) δ^{202}Hg vs. Δ^{199}Hg of the Mt. Amiata cinnabar and of the Farma Schist of the Tuscan Metamorphic Complex. (**b**) Same data in comparison with data by Pribil et al. (2020) for sediments, soils, calcine, geothermal fluid, geothermal precipitate, and ore deposits of Mt. Amiata. The symbols denoting individual deposits in this figure are the same as those of Figs. 7 and 8. The cross at the side of this and other plots shows analytical precision

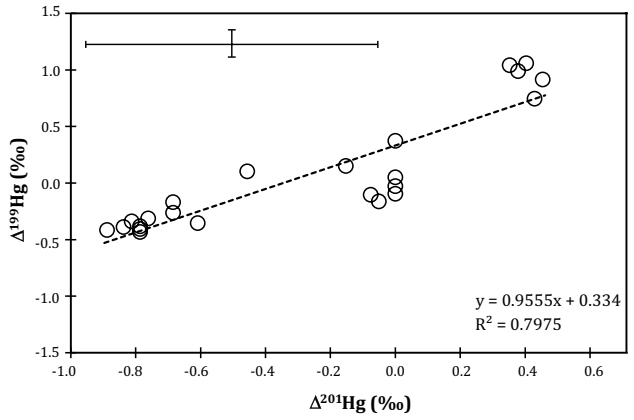

Fig. 5 Binary diagram of Δ^{199}Hg vs. Δ^{201}Hg for all samples studied. Magnitude and direction of this correlation can be used to support the hypothesis of MIF by photodegradation or other anomalies

Morone, Cortevecchia, Bàgnore, Monte Labbro, and Cornacchino) show Δ^{199}Hg between −0.35 and +1.06‰. The two samples of the Paleozoic Farma Schist show a total Hg (THg) concentration of 229 and 327 µg/kg, respectively.

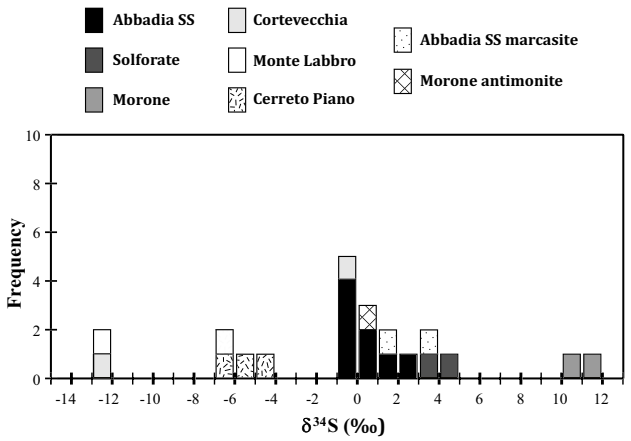

Fig. 6 Sulfur isotope compositions of cinnabar, marcasite and stibnite from the Mt. Amiata geothermal system. Marcasite and stibnite analyses are singled out (cf. Table 2)

They have δ^{202}Hg values of −3.61 and −2.94‰, and Δ^{199}Hg of −0.45 and −0.03‰, respectively (Fig. 4a).

Notably, all the cinnabar samples display a positive correlation between Δ^{199}Hg and Δ^{201}Hg with a slope that is very close to one (Fig. 5).

Fourteen out of 22 cinnabar, stibnite, and marcasite samples (from Abbadia S. Salvatore, Morone, and Cortevecchia) have δ^{34}S between −0.9 and +5‰ (Fig. 6). The other samples show compositions that are either significantly enriched (Morone) or significantly depleted in ^{34}S (Cortevecchia, Cerreto Piano, Monte Labbro). The entire δ^{34}S interval varies between −12.8 and +11.6‰.

Discussion

Fractionation processes at Mt. Amiata

The interpretation of our dataset is challenged by the fact that Hg may undergo many types of isotope fractionation generated by distinct biotic and abiotic chemical processes (Bergquist and Blum 2009; Blum et al. 2014). These include MDF induced by boiling of hydrothermal fluids, near surface oxidation, and kinetic effects associated with mineral precipitation (Smith et al. 2005, 2008), kinetic evaporation (Estrade et al. 2009; Ghosh et al. 2013), reduction of Hg(II) to elemental Hg(0) in terrestrial and marine environments (Lamborg et al. 2021; Schwab et al. 2023), and adsorption onto mineral surfaces (Jiskra et al. 2012; Schwab et al. 2023). These may be coupled with MIF produced by photochemical reduction of Hg^{2+} under natural sunlight and by photodegradation of methylmercury species in the presence of organic matter (Bergquist and Blum 2007). Notably, experiments carried out by Zheng and Hintelmann (2010a) showed that photochemical reduction of Hg(II) bound to

thiol ligands (i.e., "soft" organosulfur compounds that are abundant in the surface environment and that can bind to "soft" metal atoms like Hg) can cause *negative* MIF in the fractionated species. This mechanism was used to explain the negative MIF measured in terrestrial foliage, lichens, and moss (Blum et al. 2014), which are considered proxies of terrestrial sediments rich in organic matter. Indeed, terrestrial sediments rich in organic matter have negative Δ^{199}Hg while marine sediments show positive Δ^{199}Hg values. For instance, the documented Δ^{199}Hg of continental soil is −0.30 ± 0.05‰ (Demers et al. 2013) and that of peatland is −0.33 ± 0.11‰ (Woerndle et al. 2018). Seawater has Δ^{199}Hg of 0.14 ± 0.15‰ (Štrok et al. 2015) and marine sediments have an average Δ^{199}Hg value of 0.37 ± 0.06‰ (Meng et al. 2019).

Abiotic and biotic processes may trigger significant Hg isotope fractionation (> 1‰), depending on the type of process. The first experimental studies showed that MDF as large as 3‰ is possible in natural environments, and that large MIF (> 0.3‰) is essentially controlled by photochemical processes (Bergquist and Blum 2009; and ref. therein). However, later experimental evidence showed that MIF may take place together with MDF also in absence of light by abiotic non-photochemical reduction of Hg(II) via the mediation of dissolved organic matter (Zheng and Hintelmann 2010b). These results show, on one hand, that a complex suite of processes may control the Hg isotopic signature of a given geological environment. On the other hand, they also show that many transformations of Hg species (both organic and inorganic) need to be fully understood before Hg isotope geochemistry can be optimized to constrain the Hg cycle in detail.

In summary, current knowledge shows that MDF and MIF of Hg in natural environments produce specific Δ^{199}Hg, Δ^{201}Hg, and δ^{202}Hg values in solid, liquid and vapor species, and that Δ^{199}Hg/Δ^{201}Hg and Δ^{199}Hg/δ^{202}Hg ratios can be diagnostic of the type of reactions. Thus, photochemical reduction of Hg(II) to Hg(0) generates a Δ^{199}Hg/δ^{202}Hg of 1.00 ± 0.01 (Bergquist and Blum 2007), kinetic evaporation of Hg(0) produces a Δ^{199}Hg/δ^{202}Hg with a slope of about 0.1 (Estrade et al. 2009; Ghosh et al. 2013), and abiotic non-photochemical reduction of inorganic Hg(II) gives Δ^{199}Hg/Δ^{201}Hg between 1.5 and 1.6 (Zheng and Hintelmann 2010b). These findings show that, despite some limitations due to the lack of comprehensive experimental data, Δ^{199}Hg, Δ^{201}Hg, and δ^{202}Hg may be used to identify some useful constraints on the geological and biogeochemical processes that fractionate Hg in the environment.

In the Mt. Amiata geothermal system, the ranges of Hg isotopic compositions allow distinctions between MDF and MIF. The 3.8‰ range of δ^{202}Hg determined for the eight ore deposits (Fig. 4a, δ^{202}Hg between −3.6 and 0.17‰) is among the largest reported in the literature for mineral deposits (Blum et al. 2014) and is also very close to that of the California Coast Range cinnabar deposits (Smith et al. 2008, δ^{202}Hg between −3.88 and 0.9‰) and of the epithermal gold deposits in Nevada (δ^{202}Hg between −3.5 and 2.2‰, Smith et al. 2005). This suggests that the Mt. Amiata deposits and those of the W United States – which are both continental geothermal systems – might have formed by similar fractionation processes. In the Coast Range deposits, the clastic sedimentary rocks (Franciscan Complex, Great Valley Sequence) intruded by the local volcanic sequence (Clear Lake volcanics) were considered the source rocks of the cinnabar ore and MDF was interpreted to occur during phase separation (boiling), reduction, and volatilization of Hg species of the geothermal fluid in the near surface environment (Smith et al. 2005, 2008). We propose that the range of δ^{202}Hg found in the cinnabar of Mt. Amiata is also a combination of these processes, which have mostly fast kinetics and are therefore prone to generate lower δ^{202}Hg (Blum et al. 2014).

The Hg and S sources

The Δ^{199}Hg/Δ^{201}Hg ratio of the sample analyzed is close to 1 for the entire dataset (Fig. 5) and is comparable to the experimentally-determined Δ^{199}Hg/Δ^{201}Hg = 1 for photochemical reduction of Hg(II) to Hg(0) (Bergquist and Blum 2007). This similarity suggests that this feature is an inherited signature from the Mt. Amiata source rocks, which retained this Δ^{199}Hg/Δ^{201}Hg ratio at the time of their formation. The same feature was documented in several types of ore deposits, including the sediment-hosted (mostly Mississippi Valley Type) Pb-Zn district of Lanping, SW China (Liu et al. 2021) and the currently forming massive sulfide mineralization of the southwestern Indian ridge (Zhu et al. 2020), for which variable sources of Hg were proposed.

The relatively large MIF of the samples analyzed, which show positive and negative values, provides an indication of the heterogeneity of the source rocks of Mt. Amiata and warrant detailed evaluation. The Δ^{199}Hg vales of the Abbadia S. Salvatore, Morone, Solforate, Monte Labbro, Cortevecchia, and Cerreto Piano samples range between −0.43 and +0.37‰ (Fig. 4a), while those for Cornacchino and Bàgnore are between 0.75 and 1.06‰. Following previous work documenting MIF in sediments from marine and continental environments (Štrok et al. 2015; Woerndle et al. 2018; Meng et al. 2019; Sonke et al. 2023), we suggest that the positive MIF shown by the samples from Cornacchino, Bagnore, and Monte Labbro reflects a signature inherited from the marine sedimentary sequences present at depth in the geothermal system (rocks belonging to the Tuscan and Ligurian nappes, Figs. 1 and 2). In contrast, the relatively

large and negative MIF (Δ^{199}Hg: −0.43 to −0.31‰) displayed by cinnabar from Cortevecchia and Cerreto Piano indicate an inherited signature from terrestrial source rocks rich in organic matter, which are abundant within the thrusted-and-folded structure of the Apennines. Such lithologies may be found in the Tuscan Metamorphic Complex, which is a typical reservoir rock of the geothermal system and of which the Farma Schist is a representative lithology. The Farma Schist shows negative MIF (Δ^{199}Hg between −0.45 and −0.03‰) and THg concentrations (229–327 µg/kg) that are at least one order of magnitude higher than that of the upper continental crust (13.5 ± 17.8 ng/g, Tian et al. 2023). These compositions strongly indicate that greywacke, siltstone, and graphite-rich phyllite of continental derivation making the Tuscan Metamorphic Complex may represent significant source rocks of Hg of the geothermal system, and that several ore deposits inherited its signature to variable degrees.

Additional evidence for a heterogeneous metal source is provided by the range of δ^{34}S of cinnabar, stibnite, and marcasite from Mt. Amiata (Fig. 6), which indicates variable S sources from the hydrothermal system. A typical mantle or magmatic signature (Ohmoto and Rye 1979; Ohmoto and Goldhaber 1997) is indicated by the range of −0.9 to +3.5‰ δ^{34}S of cinnabar, stibnite, and marcasite from Abbadia San Salvatore and Morone (cf. Table 2). In contrast, the negative δ^{34}S values for the cinnabar from Cortevecchia (−12.8‰); Monte Labbro (−12.5 to −6.9‰), and Cerreto Piano (−6.8 to −4.65‰) suggest that in these deposits a proportion of S was derived from sediments rich in organic matter. The positive δ^{34}S of the cinnabar from Morone (10.1 and 11.6‰) suggests that a proportion of S was derived from marine sediments.

In synthesis, the constraints provided by the S isotopes can be combined with those provided by Δ^{199}Hg to discriminate source rock signatures at Mt. Amiata (Fig. 7). Accordingly, specific ranges of Δ^{199}Hg and δ^{34}S identify pairs of isotope compositions that define the primitive mantle, other magmatic rocks (i.e., oceanic crust, hot spot lavas, etc.), sediments, soil, and vegetation (Ohmoto and Goldhaber 1997; Demers et al. 2013; Štrok et al. 2015; Woerndle et al. 2018; Meng et al. 2019; Tian et al. 2023). These Hg-S reservoir compositions may serve as indicators of source rock signatures, while significant deviations from these compositions might indicate mixed signatures (Blum et al. 2014).

A comparison between the distribution of the Mt. Amiata Δ^{199}Hg-δ^{34}S isotope pairs and those of global reservoirs (Fig. 7) indicates that four distinct sources probably contributed to the genesis of the deposits, namely primitive mantle, continental sediments rich in organic matter and sulfides, and marine sediments. It is important to note that the Δ^{199}Hg-δ^{34}S pair of continental sediments of Fig. 7 is representative of the Farma Schist, whose Δ^{199}Hg values range from −0.39 to −0.03‰. Accordingly, the cinnabar of Abbadia S. Salvatore (the largest deposit of the district) shows ranges of Δ^{199}Hg and δ^{34}S compositions that are consistent with a derivation from the mantle, i.e. the Mt. Amiata pluton. In contrast, the pairs representing Solforate, Cerreto Piano, and Cortevecchia indicate a significant mantle derivation of S, but with variable proportions of Hg derived from continental sediments rich in organic matter. This is consistent with the depositional environment of the sandstones hosting Cerreto Piano, which belong to a transitional fluvial-coastal-shallow marine environment (Zucchetti 1964b; Dominici et al. 2018). The Δ^{199}Hg-δ^{34}S pairs of cinnabar from Morone (a deposit that contributed to c. 6% of the total Hg production of the mine district) are

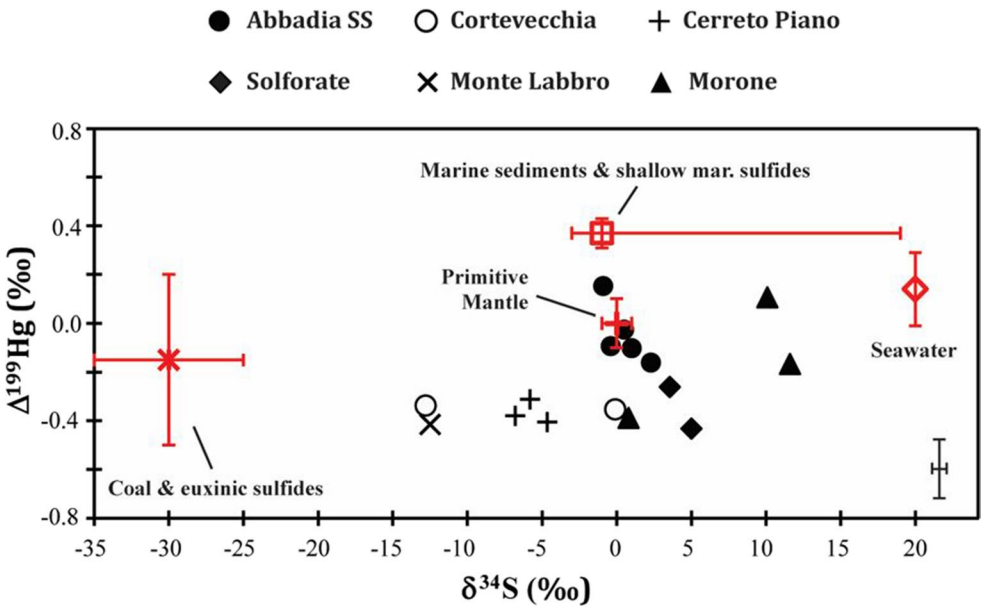

Fig. 7 Comparison between the Δ^{199}Hg and δ^{34}S ranges of the Mt. Amiata samples and those of typical Earth reservoirs. Note that the Hg and S isotopic compositions of each sample were determined from contiguous aliquots of the same sample volume. Data on S reservoirs are from Ohmoto and Rye (1979) and those on Δ^{199}Hg are from Blum et al. (2014), Tian et al. (2023), Štrok et al. (2015), (Demers et al. 2013), (Woerndle et al. 2018), and (Meng et al. 2019). Note the large δ^{34}S spread of shallow marine sediments, which is skewed towards positive values (sulfate reduction following a Rayleigh process)

significant because they indicate mixed Hg and S sources from the primitive mantle, seawater, and marine sediment, with minor input from continental sediments.

Finally, our findings confirm and integrate previous conclusions on Hg mobility in the Mt. Amiata environment (Pribil et al. 2020), which identified photochemical reduction as the process that was responsible for the Hg isotopic signature of the geothermal precipitate. A comparison between our data and those of Pribil et al. (Fig. 4b) confirms their result whereby δ^{202}Hg and Δ^{199}Hg of cinnabar, sediments, soils, geothermal water, geothermal precipitate, and calcines were controlled by the isotopic signature of the primary ore. In particular, the evidence for MIF of the geothermal water and precipitate being indistinguishable from those of the primary ore provides a strong indication that at Mt Amiata the isotopic signature of the geothermal fluid did not change with time since the inception of ore deposition and represents a source feature independent of sub-recent supergene processes.

Mt. Amiata versus other geothermal systems

There are two other major Hg districts of global importance in Europe (Blum et al. 2014). These are the districts of Almadén, Spain (Higueras et al. 2005, 2013) and Idrija, Slovenia (Palinkaš et al. 2004). Together with Mt Amiata, these districts produced > 0.5 Mt of Hg (Table 3), which corresponds to c. 50% of the historical world production (Hylander and Meili 2003). The most striking difference between Mt. Amiata, Almadén, and Idrija is represented by their δ^{202}Hg and Δ^{199}Hg ranges, which are large for Mt. Amiata but significantly narrower for Almadén and Idrija (Fig. 8; Table 3). This difference indicates that distinct source rocks and fractionation processes were responsible for the formation of cinnabar in these deposits. In the giant Almadén deposit, the c. 2‰ range of δ^{202}Hg coupled with Δ^{199}Hg 0.00 to −0.12‰ (Gray et al. 2013) relates to a submarine magmatic-hydrothermal fluid system, which formed the early stratiform and the later discordant ore bodies along diatremes of alkali-basaltic composition (Hernández et al.

Table 3 Summary of isotopic constraints on several Hg ore districts

Ore deposit	Production \ t Hg	Mineral Assemblage	δ^{202}Hg \ ‰	Δ^{199}Hg \ ‰	δ^{34}S sulfides \ ‰	Origin of Hg	Origin of S	Reference
Mt. Amiata, Italy	117,000	Cinnabar, metacinnabar, Hg(l), marcasite, stibnite	(cinn) −3.64 ÷ 0.17	(cinn) −0.43 ÷ 1.06	(cinn) −12.8 ÷ + 11.6; (marc) + 1.5 ÷ + 3.5; (stib) 0.8	Magmatic, Tuscan Metamorphic Complex; Marine sediments	Magmatic, Tuscan Metamorphic complex; Marine sediments	This study
Almadén, Spain	c. 250,000	Cinnabar, metacinnabar, Hg(l), pyrite	(cinn) −0.92 ÷ 0.15; (Hg_l) −1.36 ÷ 0.26	(cinn) −0.12 ÷ −0.08; (Hg_l) −0.31 ÷ 0.15	(cinn) 0.2 ÷ 5.9	Magmatic	Magmatic; Sea water	Gray et al. (2013); Saupé and Arnold (1992); Higueras et al. (2013)
Idrija, Slovenia	145,000	Cinnabar, Hg(l)	(cinn) −1.35 ÷ 0.53; (Hg_l) −0.89 ÷ −0.44;	(cinn) −0.18 ÷ 0.16; (Hg_l) 0.11 ÷ 0.14	(cinn) + 0.7 ÷ + 1.5 (cinn) −19.1 ÷ + 22.8; (py) −22.4 ÷ + 59.6	Magmatic	Magmatic, Thermo-chemical sulfate reduction; Sea water; Diag. Sulfides; Organic compounds	Božič et al. (2023); Lavrič and Spangenberg (2003); Palinkaš et al. (2004)
New Idria, USA	-	Unroasted cinnabar waste	−0.26 ÷ + 0.16	−0.05 ÷ 0.03	-		-	Wiederhold et al. (2013)
Calif. Coast Ranges, USA	8,900	Cinnabar	(cinn) −3.88 ÷ + 0.8	-	(cinn) + 1.53 ÷ + 7.4	Franciscan Complex/Great Valley metasediments	Magmatic; Franciscan Complex	Smith et al. (2005; 2008); Sherlock et al. (1993)

Except for the Mt. Amiata dataset, all the δ^{202}Hg, Δ^{199}Hg, and δ^{34}S data refer to distinct samples

The reported δ^{202}Hg, Δ^{199}Hg, and δ^{34}S values denote the maximum ranges of individual ore bodies, or maximum ranges of deposits from a single district, reported in the literature. Total production data should be considered lower estimates of Hg deposition in the ore environments

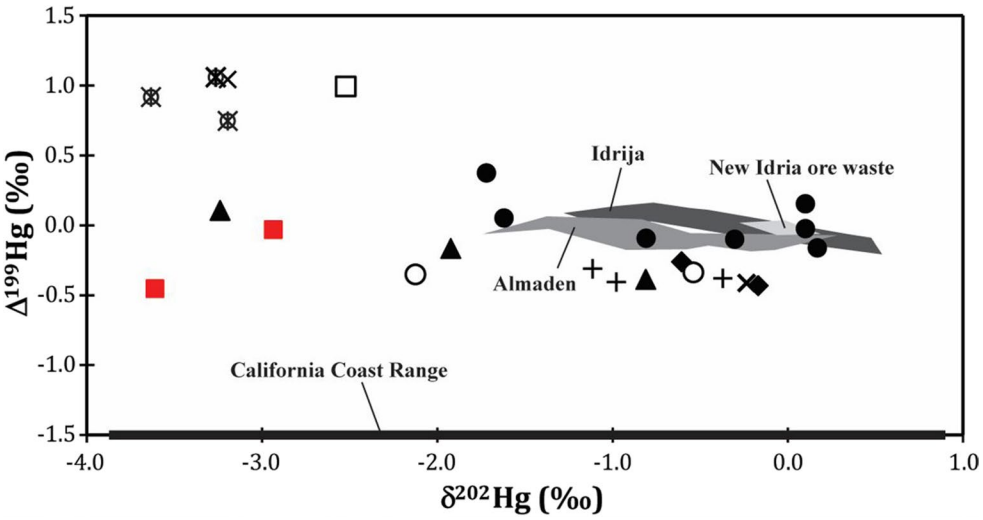

Fig. 8 Comparison between the MIF (Δ^{199}Hg) and MDF (δ^{202}Hg) data of the Mt. Amiata cinnabar and those of other mercury deposits of Europe (Almadén, Spain; Idrija, Slovenia) and of the California Coast Ranges. Data are from Smith et al. (2008), Gray et al. (2013), Wiederhold et al. (2013), and Božič et al. (2023). The thick line at the x axis denotes the reported δ^{202}Hg range of the California Coast Range deposits, for which no Δ^{199}Hg data are available. The data on the New Idria deposit, which belongs to the California Coast Range, are reported separately because they refer to mineral waste (cf. Table 3)

1999). This signature is consistent with the existence of a unique, large, and homogeneous Hg source, which can be the lower Silurian-Devonian mantle as suggested by some authors (Higueras et al. 2005, 2013). The c. 6‰ range of δ^{34}S of this cinnabar (Table 3) is consistent with mixed magmatic-sea water contributions of S to the bulk sulfide composition. Similar conclusions may be drawn for the Hg isotopic composition of cinnabar from the Idrija district (Fig. 8), which has a δ^{202}Hg range of < 2‰ and Δ^{199}Hg of −0.18 to 0.14‰ (Božič et al. 2023). These signatures are consistent with ore formation from a magmatic-hydrothermal fluid that formed the early stratiform and the later discordant ore bodies during the middle Triassic, and the δ^{34}S values are consistent with S being derived from a variety of sources (Lavrič and Spangenberg 2003).

The large ranges in δ^{202}Hg of 3.8‰, Δ^{199}Hg of 1.5‰,, and δ^{34}S of 24‰ for ore samples from Mt. Amiata, contrast with those of Almadén and Idrija. Similar large ranges were measured in the hot-spring ore deposits of the California Coast Ranges (Sherlock et al. 1993; Smith et al. 2005, 2008; Wiederhold et al. 2013). The significant differences between these districts can be explained by the range of processes that are expected to occur in submarine vs. continental geothermal systems, i.e., in the geological environments in which Almadén and Idrija on one hand, and the Mt. Amiata and Coast Range mine districts on the other hand, were generated. Both Almadén and Idrija formed in submarine geothermal systems fed by magmatic-hydrothermal fluids (Lavrič and Spangenberg 2003, and ref. therein; Higueras et al. 2013) for which δ^{202}Hg < 2‰ and small Δ^{199}Hg are known and documented (Sherman et al. 2009). In contrast, Mt. Amiata and the California Coast Range deposits are products of continental geothermal systems that formed within orogenic belts in the presence of several potential source rocks that might have provided distinct MIF and δ^{34}S signatures.

Conclusions

In the Mt. Amiata geothermal system, the isotopic compositions of Hg and S of cinnabar and other sulfides provide some useful constraints on source rock signatures and fractionation processes. Mt. Amiata is an example of a world-class continental geothermal system in which a heterogeneous source region dominated by mantle and other source rocks of continental and marine derivation, as well as hydrothermal fractionation, were functional to determining the broad ranges of Hg and S isotopic compositions. These signatures differ significantly from those of the other world-class submarine geothermal systems (Almadén and Idrija) and indicate that Hg cycling in geothermal systems occurs differently in continental and submarine environments.

Supplementary Information The online version contains supplementary material available at https://doi.org/10.1007/s00126-025-01382-8.

Acknowledgements Dr. I. Albino is gratefully acknowledged for her invaluable help during all procedures of sample preparation. We thank an anonymous reviewer and the Chief Editor Bernd Lehmann for their comments on the manuscript, which improved significantly the first versions of our work.

Author contributions Paolo S Garofalo, Orlando Vaselli, and Daniele Rappuoli contributed to the design and conceptualization of the project. Paolo S Garofalo, Simone Beccari, Daniele Rappuoli, and Gaetano Pedone carried out sample selection. Lisa Lancellotti and Andrea Marchetti contributed to the isotope data acquisition. Paolo S Garofalo, Orlando Vaselli, Lisa Lancellotti, Andrea Marchetti, and Farshid Kiani contributed to the data analysis/interpretation. The manuscript and supplementary files were produced by Paolo S Garofalo, Orlando

Vaselli, Andrea Marchetti, Lisa Lancellotti, and Farshid Kiani. The manuscript was revised and approved by all authors prior to submission.

Funding Open access funding provided by Alma Mater Studiorum - Università di Bologna within the CRUI-CARE Agreement. This work was supported by funding from the Parco Nazionale Museo delle Miniere del Monte Amiata, which is gratefully acknowledged.

Data availability The manuscript tables report all the data discussed in this manuscript and additional details are available in the Supplementary Information.

Declarations

Conflict of interest The authors declare no conflict of interest.

References

Acocella V (2000) Space accommodation by roof lifting during pluton emplacement at Amiata (Italy). Terra Nova 12(4):149–155. https://doi.org/10.1046/j.1365-3121.2000.00286.x

Acocella V, Mulugeta G (2001) Surface deformation induced by Pluton emplacement: the case of Amiata (Italy) Physics and chemistry of the earth, part. Solid Earth Geodesy 26(4):355–362. https://doi.org/10.1016/S1464-1895(01)00065-5

Agostini M (2018) Petrochemical characterization of the geological units of the Larderello geothermal field (central Italy): a possible approach for a geothermal modeling, Dipartimento di Scienze della Terra. University of Florence, Florence, Italy, p 185

Arisi Rota F, Brondi A, Dessau G, Franzini M Monte Amiata SpA, Stabilimento Minerario del Siele SpA, Stea B, Vighi L (1971) I Giacimenti Minerari, in: SIMP (Ed.) La Toscana Meridionale. Società Italiana di Mineralogia e Petrologia, pp. 357–571

Baccos F (1967) Osservazioni geologico-minerarie e genetiche sui giacimenti cinabriferi di Vallalta (Alpi Dolomitiche) e di Bagnore (Monte Amiata), Giornata di studi geominerari. Arti Grafiche Saturnia, Trento, Agordo, Italy, pp 67–112

Barelli A, Ceccarelli A, Dini I, Fiordelisi A, Giorgi N, Lovari F, Romagnoli P (2010) A review of the mt. Amiata geothermal system (Italy). World Geothermal Congress 2010. Bali, Indonesia, pp 1–6

Barnes HL (2015) Hydrothermal processes: the development of geochemical concepts in the latter half of the twentieth century. Geochem Perspect 4:1–93

Barnes HL, Seward TM (1997) Geothermal systems and mercury deposits. In: Barnes HL (ed) Geochemistry of hydrothermal ore deposits. Wiley, pp 699–736

Batini F, Brogi A, Lazzarotto A, Liotta D, Pandeli E (2003) Geological features of Larderello-Travale and Mt. Amiata geothermal areas (southern Tuscany, Italy). Episodes 26(3):239–244

Bergquist BA, Blum JD (2007) Mass-dependent and -independent fractionation of Hg isotopes by photoreduction in aquatic systems. Science 318(5849):417–420. https://doi.org/10.1126/science.1148050

Bergquist BA, Blum JD (2009) The odds and evens of mercury isotopes: applications of mass-dependent and mass-independent isotope fractionation. Elements 5(6):353–357. https://doi.org/10.2113/gselements.5.6.353

Bertani R (2016) Geothermal power generation in the world 2010–2014 update report. Geothermics 60:31–43. https://doi.org/10.1016/j.geothermics.2015.11.003

Blum JD, Sherman LS, Johnson MW (2014) Mercury isotopes in Earth and environmental sciences. Annu Rev Earth Planet Sci 42(1):249–269. https://doi.org/10.1146/annurev-earth-050212-124107

Bonciani F, Callegari I, Conti P, Cornamusini G, Carmignani L (2005) Neogene post-collisional evolution of the internal Northern apennines: insights from the upper Fiora and Albegna valleys, (Mt. Amiata geothermal area, Southern Tuscany). Bollettino Della Società Geologica Italiana Vol Spec 3:103–118

Božič D, Živković I, Dizdarević T, Peljhan M, Štrok M, Horvat M (2023) Insights into the heterogeneity of the mercury isotopic fingerprint of the Idrija mine (Slovenia). Minerals 13(9):1227

Brogi A (2008) The triassic and palaeozoic successions drilled in the Bagnore geothermal field and Poggio Nibbio area (Monte Amiata, Northern Apennines, Italy). Ital J Geosci 127(3):599–613

Brown KL, Simmons SF (2003) Precious metals in high-temperature geothermal systems in New Zealand. Geothermics 32(4–6):619–625. https://doi.org/10.1016/S0375-6505(03)00049-X

Cadoux A, Pinti DL (2009) Hybrid character and pre-eruptive events of Mt Amiata volcano (Italy) inferred from geochronological, petro-geochemical and isotopic data. J Volcanol Geotherm Res 179(3):169–190. https://doi.org/10.1016/j.jvolgeores.2008.10.018

Calamai A, Cataldi R, Squarci P, Taffi L (1970) Geology, geophysics and hydrogeology of the Monte Amiata geothermal field. Geothermics 1(Special Issue 1):1–9

Carmignani L, Decandia FA, Fantozzi PL, Lazzarotto A, Liotta D, Meccheri M (1994) Tertiary extensional tectonics in Tuscany (Northern apennines, Italy). Tectonophysics 238:295–315

Cassinis R, Scarascia S, Lozej A (2005) Review of seismic Wide-Angle Reflection-Refraction (WARR) results in the Italian region (1956–1987). In: Finetti IR (ed) CROP PROJECT: deep seismic exploration of the central mediterranean and Italy. Elsevier, pp 31–55

Cataldi R (1967) Remarks on the geothermal research in the region of Monte Amiata (Tuscany - Italy). Bull Volcanol 30(1):243–269. https://doi.org/10.1007/BF02597673

Chiarabba C, Amato A, Fiordelisi A (1995) Upper crustal tomographic images of the Amiata-Vulsini geothermal region, central Italy. J Geophys Res: Solid Earth 100(B3):4053–4066. https://doi.org/10.1029/94JB02870

Conticelli S, Laurenzi M, Giordano G, Mattei M, Avanzinelli R, Melluso L, Tommasini S, Boari E, Cifelli F, Perini G (2010) Leucite-bearing (kamafugitic/leucititic) and -free (lamproitic) ultrapotassic rocks and associated shoshonites from italy: constraints on petrogenesis and geodynamics. J Virtual Explorer 36. https://doi.org/10.3809/jvirtex.2010.00251

Conticelli S, Boari EL, Burlamacchi L, Cifelli F, Moscardi F, Laurenzi MA, Ferrari Pedraglio L, Francalanci L, Benvenuti MG, Braschi E, Manetti P (2015) Geochemistry and Sr-Nd-Pb isotopes of Monte Amiata volcano, central Italy: evidence for magma mixing

between high-K calc-alkaline and leucititic mantle-derived magmas. Ital J Geosci 134(2):266–290. https://doi.org/10.3301/IJG.2015.12

Cornamusini G, Foresi LM, Massa G, Bonciani F, Callegari I, Da Prato S, Ielpi A (2011) The Miocene successions of the Fiora hills: considerations about the development of the minor basins of Southern Tuscany. Ital J Geosci 130:404. https://doi.org/10.3301/IJG.2011.17

Davey HA (1974) Mechanism for mercury deposition at Ngawha Springs, New Zealand. Pap Proc R Soc Tasmania 108:157–158

De Castro C (1914) Genesi dei giacimenti cinabriferi del Monte Amiata, Memorie Descrittive Carta Geologica d'Italia. pp. 1–77

De Ferrari P (1890) Le miniere Di mercurio Del Monte Amiata. Tipografia Garbera Firenze

Della Vedova B, Bellani S, Pellis G, Squarci P (2001) Deep temperatures and surface heat flow distribution. In: Vai GB, Martini IP (eds) Anatomy of an orogen: the Apennines and adjacent mediterranean basins. Springer Netherlands, Dordrecht, pp 65–76. https://doi.org/10.1007/978-94-015-9829-3_7

Demers JD, Blum JD, Zak DR (2013) Mercury isotopes in a forested ecosystem: implications for air-surface exchange dynamics and the global mercury cycle. Glob Biogeochem Cycles 27(1):222–238. https://doi.org/10.1002/gbc.20021

Dominici S, Danise S, Benvenuti M (2018) Pliocene stratigraphic paleobiology in Tuscany and the fossil record of marine megafauna. Earth Sci Rev 176:277–310. https://doi.org/10.1016/j.earscirev.2017.09.018

Elter FM, Pandeli E (1991) Structural features of the metamorphic Paleozoic-Triassic sequences in deep geothermal drillings of the Monte Amiata area (SE Tuscany, Italy). Ital J Geosci 110(3–4):511–522

Engelbrecht H (2008) Carboniferous continental margin deposits in southern Tuscany, Italy: results from geological mapping of the geotopes Farma Valley and San Antonio mine area. Geol J 43(2–3):279–305. https://doi.org/10.1002/gj.1106

Estrade N, Carignan J, Sonke JE, Donard OFX (2009) Mercury isotope fractionation during liquid–vapor evaporation experiments. Geochim Cosmochim Acta 73(10):2693–2711. https://doi.org/10.1016/j.gca.2009.01.024

Faccenna C, Becker TW, Lucente FP, Jolivet L, Rossetti F (2001) History of subduction and back arc extension in the central Mediterranean. Geophys J Int 145(3):809–820. https://doi.org/10.1046/j.0956-540x.2001.01435.x

Forconi S (2011) Il Cinabro Sul Monte amiata. Giacimenti, impianti di trasformazione ed organizzazione del lavoro. Edizioni HgS, Abbadia S. Salvatore

Fulignati P, Marianelli P, Sbrana A, Ciani V (2014) 3D Geothermal Modelling of the Mount Amiata Hydrothermal System in Italy. Energies 7(11):7434–7453

Ghosh S, Schauble EA, Lacrampe Couloume G, Blum JD, Bergquist BA (2013) Estimation of nuclear volume dependent fractionation of mercury isotopes in equilibrium liquid–vapor evaporation experiments. Chem Geol 336:5–12. https://doi.org/10.1016/j.chemgeo.2012.01.008

Gianelli G, Puxeddu M, Batini F, Bertini G, Dini I, Pandeli E, Nicolich R (1988) Geological model of a young volcano-plutonic system: the geothermal region of Monte Amiata (Tuscany, Italy). Geothermics 17(5/6):719–734

Gray JE, Pribil MJ, Higueras PL (2013) Mercury isotope fractionation during ore retorting in the Almadén mining district, Spain. Chem Geol 357:150–157. https://doi.org/10.1016/j.chemgeo.2013.08.036

Hardardóttir V, Hannington M, Hedenquist J (2013) Metal concentrations and metal deposition in deep geothermal wells at the Reykjanes High-temperature area, Iceland. Procedia Earth Planet Sci 7:338–341. https://doi.org/10.1016/j.proeps.2013.03.159

Hedenquist JW, Lowenstern JB (1994) The role of magmas in the formation of hydrothermal ore deposits. Nature 370(6490):519–527

Hernández A, Jébrak M, Higueras P, Oyarzun R, Morata D, Munhá J (1999) The Almadén mercury mining district, Spain. Miner Deposita 34:539–548

Higueras P, Munhá J, Oyarzun R, Tassinari CCG, Ruiz IR (2005) First lead isotopic data for cinnabar in the Almadén district (Spain): implications for the genesis of the mercury deposits. Miner Deposita 40(1):115–122. https://doi.org/10.1007/s00126-005-0471-2

Higueras P, Oyarzun R, Lillo J, Morata D (2013) Intraplate mafic magmatism, degasification, and deposition of mercury: the giant Almadén mercury deposit (Spain) revisited. Ore Geol Rev 51:93–102. https://doi.org/10.1016/j.oregeorev.2012.12.004

Hylander LD, Meili M (2003) 500 years of mercury production: global annual inventory by region until 2000 and associated emissions. Sci Total Environ 304:13–27

Jiskra M, Wiederhold JG, Bourdon B, Kretzschmar R (2012) Solution speciation controls mercury isotope fractionation of Hg(II) sorption to goethite. Environ Sci Technol 46(12):6654–6662. https://doi.org/10.1021/es3008112

Jolivet L, Faccenna C, Goffé B, Mattei M, Rossetti F, Brunet C, Storti F, Funiciello R, Cadet JP, d'Agostino N, Parra T (1998) Midcrustal shear zones in postorogenic extension: example from the Northern tyrrhenian sea. J Geophys Res: Solid Earth 103(B6):12123–12160

Lamborg CH, Hansel CM, Bowman KL, Voelker BM, Marsico RM, Oldham VE, Swarr GJ, Zhang T, Ganguli PM (2021) Dark reduction drives evasion of mercury from the ocean. Front Environ Chem 2. https://doi.org/10.3389/fenvc.2021.659085

Lavrič JV, Spangenberg JE (2003) Stable isotope (C, O, S) systematics of the mercury mineralization at Idrija, Slovenia: constraints on fluid source and alteration processes. Miner Deposita 38(7):886–899. https://doi.org/10.1007/s00126-003-0377-9

Lepak RF, Yin R, Krabbenhoft DP, Ogorek JM, DeWild JF, Holsen TM, Hurley JP (2015) Use of stable isotope signatures to determine mercury sources in the Great Lakes. Environ Sci Technol Lett 2(12):335–341. https://doi.org/10.1021/acs.estlett.5b00277

Liu Y-F, Qi H-W, Bi X-W, Hu R-Z, Qi L-K, Yin R-S, Tang Y-Y (2021) Mercury and sulfur isotopic composition of sulfides from sediment-hosted lead-zinc deposits in Lanping basin, Southwestern China. Chem Geol 559:119910. https://doi.org/10.1016/j.chemgeo.2020.119910

Marroni M, Moratti G, Costantini A, Conticelli S, Benvenuti MG, Pandolfi L, Bonini M, Cornamusini G, Laurenzi MA (2015a) Geology of the Monte Amiata region, Southern tuscany, central Italy. Ital J Geosci 134(2):171–199. https://doi.org/10.3301/ijg.2015.13

Marroni M, Pandeli E, Pandolfi L, Catanzariti R (2015b) Updated picture of the Ligurian and Sub-Ligurian units in the mt. Amiata area (Tuscany, Italy): elements for their correlation in the framework of the Northern Apennines. Ital J Geosci 134(2):200–218. https://doi.org/10.3301/ijg.2014.47

Martini IP, Sagri M (1993) Tectono-sedimentary characteristics of late Miocene-Quaternary extensional basins of the Northern Apennines, Italy. Earth Sci Rev 34(3):197–233. https://doi.org/10.1016/0012-8252(93)90034-5

Meng M, Sun R-y, Liu H-w, Yu B, Yin Y-g, Hu L-g, Shi J-b, Jiang G-b (2019) An integrated model for input and migration of mercury in Chinese coastal sediments. Environ Sci Technol 53(5):2460–2471. https://doi.org/10.1021/acs.est.8b06329

Meyer HM, Mitchell AW (1947) Mercury in: Matthews A.F. (Ed.) Minerals Yearbook. US Geological Survey, pp. 765–778

Morteani G, Ruggieri G, Moeller P, Preinfalk C (2011) Geothermal mineralized scales in the pipe system of the geothermal Piancastagnaio power plant (Mt. Amiata geothermal area): a key to

understand the stibnite, cinnabarite and gold mineralization of Tuscany (central Italy). Miner Deposita 46(2):197–210
Ohmoto H, Goldhaber M (1997) Sulfur and carbon isotopes. In: Barnes HD (ed) Geochemistry of hydrothermal ore deposits. Wiley, pp 517–611
Ohmoto H, Rye RO (1979) Isotopes of Sulfur and Carbon. In: Barnes HD (ed) Geochemistry of hydrothermal ore deposits. Wiley, pp 509–567
Palinkaš L, Strmic Palinkas S, Spangenberg J, Prochaska W, Herlec U (2004) Ore-forming fluids in the Grubler orebody, Idrija mercury deposit, Slovenia. Swiss Bull Miner Petrol 84:173–188
Pandeli E, Puxeddu M, Gianelli G, Bertini G, Castellucci P (1988) Paleozoic sequences crossed by deep drillings in the Monte Amiata geothermal region (Italy). Boll Soc Geol Ital 107:593–606
Peccerillo A, Donati C (2003) The Tuscan Magmatic Province. Period Miner 72(Special Issue):27–39
Peccerillo A, Poli G, Donati C (2001) The plio-quaternary magmatism of Southern Tuscany and Northern Latium: compositional characteristics, genesis, and geodynamic significance. Ofioliti 26(2a):229–238
Plant JA, Bone J, Voulvoulis N, Kinniburgh DG, Smedley PL, Fordyce FM, Klinck B (2014) 11.2 - Arsenic and selenium. In: Holland HD, Turekian KK (eds) Treatise on geochemistry (Second Edition). Elsevier, Oxford, pp 13–57. https://doi.org/10.1016/B978-0-08-095975-7.00902-5.
Pribil MJ, Rimondi V, Costagliola P, Lattanzi P, Rutherford DL (2020) Assessing mercury distribution using isotopic fractionation of mercury processes and sources adjacent and downstream of a legacy mine district in Tuscany, Italy. Appl Geochem 117:104600. https://doi.org/10.1016/j.apgeochem.2020.104600
Saupé F, Arnold M (1992) Sulphur isotope geochemistry of the ores and country rocks at the Almadén mercury deposit, Ciudad Real, Spain. Geochim Cosmochim Acta 56(10):3765–3780. https://doi.org/10.1016/0016-7037(92)90169-J
Savoia U (1919) Le mini ere cinabrifere italiane. La Miniera Italiana 3(7–8):233–248
Schavecher N (1990) Studio geo-giacimentologico della zona di Bagnore (Toscana meridionale), Dipartimento di Scienze della Terra. University of Milan, Milan, Italy, p 218
Schwab L, Gallati N, Reiter SM, Kimber RL, Kumar N, McLagan DS, Biester H, Kraemer SM, Wiederhold JG (2023) Mercury isotope fractionation during dark abiotic reduction of Hg(II) by dissolved, surface-bound, and structural Fe(II). Environ Sci Technol 57(40):15243–15254. https://doi.org/10.1021/acs.est.3c03703
Segreto L (1991) Monte Amiata. Il mercurio italiano. Strategie internazionali e vincoli extraeconomici. Franco Angeli (Ed.)
Seward TM, Williams-Jones AE, Migdisov AA (2014) 13.2 - The chemistry of metal transport and deposition by Ore-Forming hydrothermal fluids. In: Holland HD, Turekian KK (eds) Treatise on geochemistry (Second Edition). Elsevier, Oxford, pp 29–57. https://doi.org/10.1016/B978-0-08-095975-7.01102-5
Sherlock RL, Amelia M, Logan V, Craig Jowett E, Rytuba JJ (1993) Silica carbonate alteration of serpentinite, implications for the association of precious metal and mercury mineralization in the Coast Ranges, in: Rytuba J.J. (Ed.) Active Geothermal Systems and Gold-Mercury Deposits in the Sonoma-Clear Lake Volcanic Fields, California. Society of Economic Geologists, pp 90–116. https://doi.org/10.5382/gb.16
Sherman LS, Blum JD, Nordstrom DK, McCleskey RB, Barkay T, Vetriani C (2009) Mercury isotopic composition of hydrothermal systems in the Yellowstone plateau volcanic field and Guaymas basin sea-floor rift. Earth Planet Sci Lett 279(1–2):86–96. https://doi.org/10.1016/j.epsl.2008.12.032
Sillitoe RH, Brogi A (2021) Geothermal systems in the Northern Apennines, Italy: modern analogues of Carlin-style gold deposits. Econ Geol 116(7):1491–1501. https://doi.org/10.5382/econgeo.4883
Simmons SF, Brown KL (2007) The flux of gold and related metals through a volcanic arc, Taupo Volcanic Zone, New Zealand. Geology 35(12):1099–1102. https://doi.org/10.1130/g24022a.1
Smith CN, Kesler SE, Klaue B, Blum JD (2005) Mercury isotope fractionation in fossil hydrothermal systems. Geology 33(10):825–828. https://doi.org/10.1130/G21863.1
Smith CN, Kesler SE, Blum JD, Rytuba JJ (2008) Isotope geochemistry of mercury in source rocks, mineral deposits and spring deposits of the California Coast Ranges, USA. Earth Planet Sci Lett 269(3–4):399–407. https://doi.org/10.1016/j.epsl.2008.02.029
Sonke JE, Shevchenko VP, Prunier J, Sun R, Prokushkin AS, Pokrovsky OS (2023) Mercury stable isotope composition of lichens and mosses from Northern Eurasia reveals Hg deposition pathways and sources. ACS Earth Space Chem 7(1):204–211. https://doi.org/10.1021/acsearthspacechem.2c00297
Strappa O (1977a) Storia delle miniere di mercurio del Monte Amiata. I Parte. L'Industria Miner XXVIII(4):252–259
Strappa O (1977b) Storia delle miniere di mercurio del Monte Amiata. II Parte. L'Industria Miner XXVIII (2):336–432
Strappa O. (1977c) Storia delle miniere di mercurio del Monte Amiata. III Parte. L'Industria Mineraria XXVIII (2), 433–439
Štrok M, Baya PA, Hintelmann H (2015) The mercury isotope composition of Arctic coastal seawater. CR Geosci 347(7):368–376. https://doi.org/10.1016/j.crte.2015.04.001
Tanelli G (1983) Mineralizzazioni metallifere e metallogenesi della Toscana. Memorie Della Società Geologica Italiana 25:91–109
Tian Z, Lehmann B, Deng C, Luo A, Zhang X, Moynier F, Yin R (2023) Mercury abundance and isotopic composition in granitic rocks: implications for Hg cycling in the upper continental crust. Geochim Cosmochim Acta. https://doi.org/10.1016/j.gca.2023.09.019
Varekamp JC, Buseck PR (1984) The speciation of mercury in hydrothermal systems, with applications to ore deposition. Geochim Cosmochim Acta 48(1):177–185. https://doi.org/10.1016/0016-7037(84)90359-4
Various Authors (2023) European Commission Study on the critical Raw materials for the EU 2023 - Final report. European Commission, Brussels, pp. 1–158
Washburn SJ, Blum JD, Kurz AY, Pizzuto JE (2018) Spatial and temporal variation in the isotopic composition of mercury in the South River, VA. Chem Geol 494:96–108. https://doi.org/10.1016/j.chemgeo.2018.07.023
White DE (1981) Active geothermal systems and hydrothermal ore deposits, Seventy-fifth Anniversary volume. Soc Economic Geol. https://doi.org/10.5382/av75.12
Wiederhold JG, Smith RS, Siebner H, Jew AD, Brown GE Jr., Kretzschmar BB (2013) Mercury isotope signatures as tracers for Hg cycling at the New Idria Hg Mine. Environ Sci Technol 47(12):6137–6145. https://doi.org/10.1021/es305245z
Woerndle GE, Tsz-Ki Tsui M, Sebestyen SD, Blum JD, Nie X, Kolka RK (2018) New insights on ecosystem mercury cycling revealed by stable isotopes of mercury in water flowing from a headwater peatland catchment. Environ Sci Technol 52(4):1854–1861. https://doi.org/10.1021/acs.est.7b04449
Zhang Z, Zhang B, Long J, Zhang X, Chen G (1998) Thallium pollution associated with mining of thallium deposits. Sci China Ser D Earth Sci 41(1):75–81. https://doi.org/10.1007/BF02932424
Zheng W, Hintelmann H (2010a) Isotope fractionation of mercury during its photochemical reduction by low-molecular-weight organic compounds. J Phys Chem A 114(12):4246–4253. https://doi.org/10.1021/jp9111348
Zheng W, Hintelmann H (2010b) Nuclear field shift effect in isotope fractionation of mercury during abiotic reduction in the absence

of light. J Phys Chem A 114(12):4238–4245. https://doi.org/10.1021/jp910353y

Zhu C, Tao C, Yin R, Liao S, Yang W, Liu J, Barriga FJ, A.S (2020) Seawater versus mantle sources of mercury in sulfide-rich seafloor hydrothermal systems, Southwest Indian Ridge. Geochim Et Cosmochim Acta 281:91–101. https://doi.org/10.1016/j.gca.2020.05.008

Zucchetti S (1964b) I giacimenti mercuriferi secondari della Toscana e l'eta della locale metallogenesi. Rend della dlasse di Scienze Fis Mat e Naturali XXXVI(5):658–668

Zucchetti S (1964a) I giacimenti cinabriferi detrici e residuali del distretto amiatino. L'Industria Mineraria XV, 465–507